NANO LETTERS

LETTER

pubs.acs.org/NanoLett

Crystallization of Fluorescent Quantum Dots within a Three-Dimensional Bio-Organic Template of Actin Filaments and Lipid Membranes

Etienne Henry,[†,‡] Aurélien Dif,[§] Marc Schmutz,[∥] Loic Legoff,[⊥] François Amblard,[⊥] Valérie Marchi-Artzner,[*,§] and Franck Artzner[*,†]

[†]Institut de Physique de Rennes, UMR 6251 CNRS, Université Rennes 1, Avenue du Général Leclerc, 35042 Rennes Cedex, France

[‡]LBPA, UMR CNRS 8113, ENS Cachan, 94235 Cachan, France

[§]Sciences Chimiques de Rennes, UMR 6226 CNRS, Université Rennes 1, Avenue du Général Leclerc, 35042 Rennes Cedex, France

[∥]Institut Charles Sadron, UPR 22 CNRS, Université de Strasbourg, 23 rue du Loess, 67034 Strasbourg, France

[⊥]Laboratoire de Physico-chimie, UMR 168 CNRS, Institut Curie, 11 rue Pierre et Marie Curie, 75248 Paris Cedex 04, France

Supporting Information

ABSTRACT: Biological molecules and molecular self-assemblies are promising templates to organize well-defined inorganic nanostructures. We demonstrate the ability of a self-assembled three-dimensional crystal template of helical actin protein filaments and lipids bilayers to generate a hierarchical self-assembly of quantum dots. Functionnalized tricystein peptidic quantum dots (QDs) are incorporated during the dynamical self-assembly of this actin/lipid template resulting in the formation of crystalline fibers. The crystal parameters, 26.5 × 18.9 × 35.5 nm^3, are imposed by the membrane thickness, the diameter, and the pitch of the actin self-assembly. This process ensures the high quality of the crystal and results in unexpected fluorescence properties. This method of preparation offers opportunities to generate crystals with new symmetries and a large range of distance parameters.

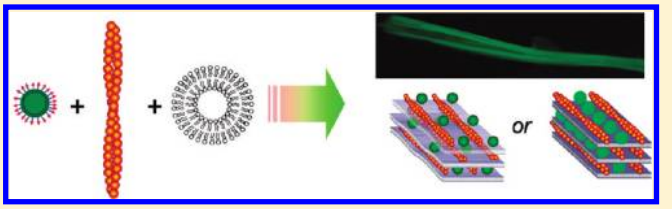

KEYWORDS: Peptidic quantum dots, actin, vesicles, hydrid self-assemblies, nanoparticle crystal

Generating new physical properties using the crystallization of nanoparticles (NPs) is highly challenging.[1−7] The design of such new materials with unexpected physical properties is thus the major motivation in the investigation of new strategies for controlling the crystallization of nanoparticles. It is now possible to produce NPs having a variety of specific optical, electronic, or magnetic properties. The couplings between their individual properties come from various interactions such as electrostatic or magnetic field, absorption dipole, wave function overlap, and so forth. The emergence of collective properties arising from such couplings has been demonstrated in the case of one-dimensional (1D) chains of NPs or two-dimensional (2D) assemblies.[5,6,8] In particular, the collective optical properties of such ensemble have been mainly attributed to the close vicinity between nanoparticles.[9] The fabrication of 3D crystalline organizations with well-defined characteristic lengths could permit to extend the coupling far away from the first neighbors so that delocalized eigenstate are expected to appear as observed with 3D crystal of atoms.[10] Moreover, as the coupling strength strongly depends on the NPs interdistance, the spatial organization of NPs, the extension, and the quality of this order should govern these new properties.[11]

Colloidal crystallization from a homogeneous suspension of spherical objects is the most effective process to produce 3D cubic structures.[1−6] NPs surface functionalization has been extensively developed in order to improve the quality of the crystal and tune the NPs interdistance. This can be achieved by surfactants, polymers, and biomolecules. Recently, double strand DNA interactions have successfully demonstrated the unique possibility to modulate the NPs interdistance.[12,13] Another strategy for NPs crystallization is based on their incorporation within three-dimensional crystal templates. Biological molecules[1] and molecular self-assemblies are promising templates to organize well-defined inorganic nanostructures.[11] This approach offers opportunities to generate crystals with new symmetries and a larger range of distance parameters. An alternative strategy consists in exploiting three-dimensional (3D) templates to synthesize NPs in situ.[14] This elegant promising method opens access to crystals with new symmetries that are hardly accessible from isotropic NPs but is restricted to NPs obtained in mild conditions excluding for example the versatile core−shell semiconductive NPs such as fluorescent QDs. Our strategy is to incorporate the NPs during the self-assembling process of a dynamical template that imposes the symmetry of the emerging NPs crystal (Scheme 1).

Received: September 15, 2011
Revised: November 8, 2011
Published: November 11, 2011

Scheme 1. Mechanism of QDs inclusion during the dynamical self-assembly of the 3D template[a]

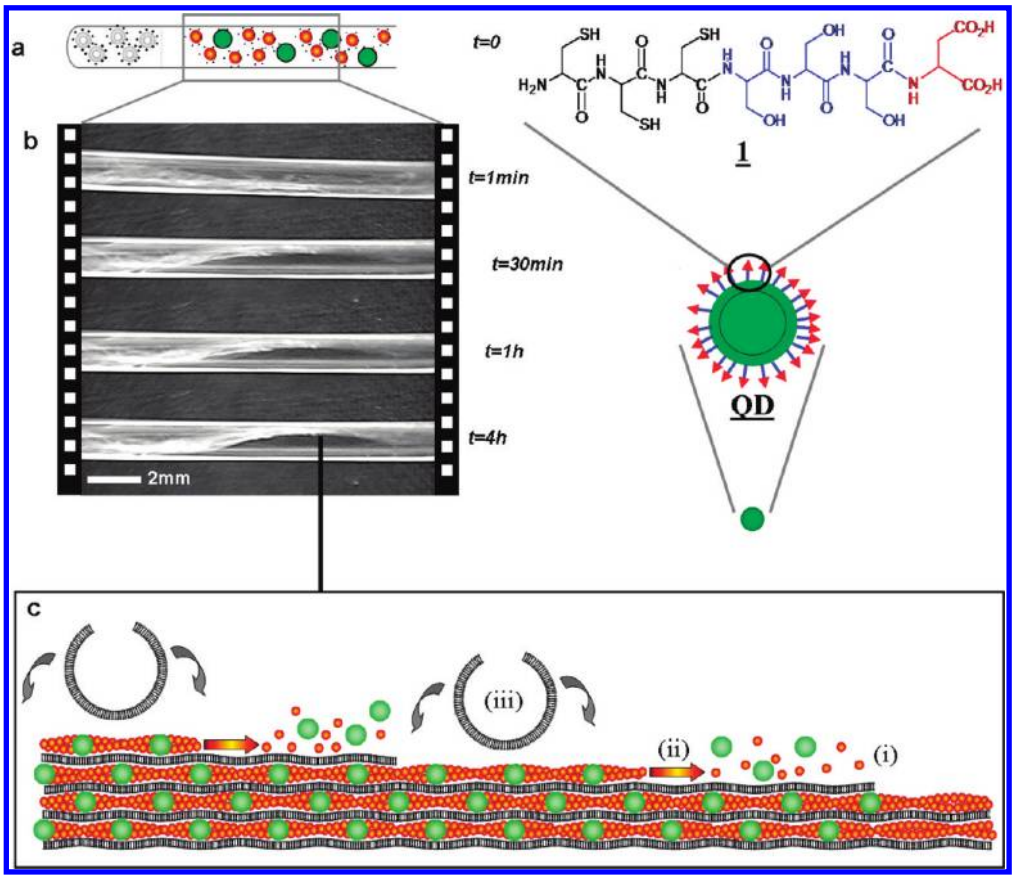

[a] Cationic vesicles (black), actin monomer (red), and quantum dots (green) are mixed in a capillary (a) and slowly self-organize into centimeter long fibrils (b). The building up of the crystal results from a three-step sequence (c): (i) the electrostatic adsorption of anionic CCCSSSD peptide **1** quantum dots QD and actin proteins onto the cationic membranes; (ii) the actin polymerisation and (iii) the rupture of cationic vesicles by adhesion onto the anionic filaments.

Here, we describe the preparation of a self-assembled 3D crystal template of helical actin protein filaments embedded within lipid bilayers (Figure 1). Functionalized peptidic quantums dots[15] (QDs) are incorporated during the self-assembling of the template[16] (Scheme 1). This process ensures the high quality of the crystal and results in specific fluorescence properties.

In a first simple approach,[15] we used lipid multilayers as a template to insert water-soluble functionalized QDs of opposite charge. Hydrophobic CdSe/ZnS quantum dots were first functionalized with a short CCCSSSD heptapeptide **1** bearing three cysteins as an anchor to the ZnS surface sequence and a C-terminal aspartic acid as anionic function according to our previous described protocols (Supporting Information 1).[15,17] As a result of attractive Coulombic interactions, a lamellar order is obtained with a spacing forced by the QD diameter (mean hydrodynamical diameter 9±1 nm).[15] Meanwhile, the in-plane order is lost, as indicated by disordered 2D corrugations. In order to recover the in-plane ordering, we included extraneous objects providing additional well-defined length scales and compatible with the lamellar structure. In these respects, the most promising objects in hand are biomolecules. Because we aim at achieving in-plane order, two length scales are required therefore actin microfilament appears to be the most appropriate choice. This biopolymer self-assembles from a globular monomer (43 kDa, ~5 nm diameter) into a left-handed helix with cross-section having a thick (8 nm) and a thin (6 nm) axes. These two length scales are closed to the diameter of the QD used in our first structure, and microfilaments should therefore be compatible with the lamellar phase reported above. The shape of the cross-section results in an effective modulation of the projected width with a 35 nm pitch. In addition, it has been shown that actin microfilaments can self-assemble on contact with lipid bilayers, leading either to paracrystal formation[18] or multilayered structures.[19] Therefore, we chose the actin microfilaments to enhance the ordering of the QD-lipid phase, first investigating the 3D template self-assembly and then optimizing the QDs incorporation.

The template (Figure 1) was prepared by the addition of monomeric actin to DMTAP/DMPC (1:9) small unilamellar vesicles, and polymerization buffer was gradually added after 30 min. The morphology observed by polarization microscopy reveals a centimeter long, strongly birefringent fiber (Figure 1a). This structure is obtained after a few days because of the slow mixing of the components in the capillary. Fiber diffraction by SAXS experiments exhibits Bragg peaks that can be interpreted as the sum of a 2D lattice and the vertical diffuse scattering (Figure 1b). The *hk* plane of the 2D lattice is centered with systematic extinction for $h + k = 2n + 1$ with cell dimensions $a = 25$ nm and $b = 38$ nm. Here b is very close to half of the helical pitch of F-actin and a is approximately twice the thickness of a superlayer made of one bilayer (4 nm) of lipids and one monolayer

dx.doi.org/10.1021/nl203216q |*Nano Lett.* 2011, 11, 5443–5448

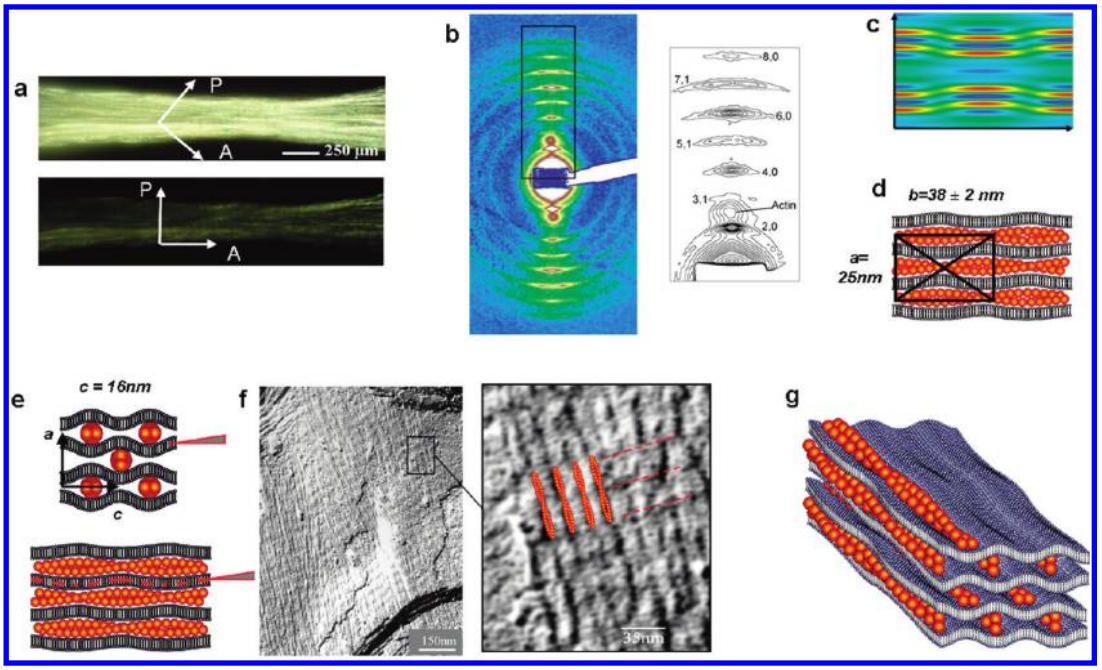

Figure 1. Structural characterization of the 3D actin/lipid crystal template composed of F-actin microfilaments layers alternating with lipid membranes and obtained by mixing DMTAP/DMPC (1:9) small unilamellar vesicles (20 mg/mL), G-actin (12 μmol/L) and gradually complementing by F-buffer. (a) Morphologies observed by polarization microscopy. (b) Fiber diffraction observed by SAXS experiments performed with a 1.5 m sample−detector distance at ID02@ESRF and the corresponding peak indexations in a centered rectangular lattice superimposed to the (1,0,1) diffuse scattering due to pair interactions between F-actin microfilaments. (c) Electron density projection on the (a,b) plane reveals peristaltic oscillation of the phosphate headgroups (yellow-red) and actin helical pitch (blue-green). (d,e) Schematic views of the structure. Strong electrostatic interactions between anionic microfilaments and cationic lipids results in large undulations of the lipid bilayers. Red wedges indicate the freeze fracture plane. (f) Freeze fracture electron microscopy between the lipid bilayers shows two perpendicular corrugations. Actin microfilaments are drawn as a scale reference. (g) Schematic sketch of the 3D organization.

of aligned in phase F-actin microfilaments (8 nm). On the basis of this, a simple and natural structural model is proposed (Figure 1d) where the unit cell perpendicular to the lipid bilayer is composed of two such superlayers, the helical phase of the F-actin microfilaments being π-shifted between adjacent superlayers. The electron density variations along the F-actin microfilaments are vanishing so that both (1,1) and (0,2) peak intensities are very low. The electron density map (Figure 1c) constructed from SAXS intensity distributions is in agreement with microfilament localization and membrane corrugations of our model. High-resolution SAXS profiles (Supporting Information S6) show an additional diffuse scattering peak which is shifted to small angles during the lipid chain melting transition from the L_β gel (q = 0.052 Å^{-1}) to the L_α fluid chain state (q = 0.049 Å^{-1}). A similar shift, also observed in DNA/DMTAP/DMPC phases, has been unambiguously attributed to the lateral dilatation of the DNA superlattice.[20,21] By analogy, this diffuse scattering is attributed to pair interactions between adjacent microfilaments that correspond to a local order along c without positional long-range order freeze fracture electron microscopy observations confirm the above model by showing egg box membrane deformations with perpendicular directions of undulation and spatial periods of 35 and 15 nm (Figure 1f). The former corresponds to an undulation of the bilayer imposed by the periodic longitudinal variation of the apparent thickness of microfilaments (Figure 1e). The latter reflects the local lateral arrangement along c of actin microfilament cross sections in the plane perpendicular to actin microfilaments (Figure 1e) with the (1,0,1) indexation of the diffuse scattering peak (Figure 1b).

To prepare QD crystals, hydrophilic QDs were added to the actin on contact with lipid biliayers by taking advantage of the slowness of the self-assembling process. The QDs were first functionalized with a negatively charged peptide **1**[15,17] so that they can interact with the cationic membranes. The anionic actin proteins (6 nm diameter) and functionalized QDs (8 nm diameter) were homogeneously mixed before addition to vesicles suspension (scheme 1). Since both polyanions (actin and QDs) are attracted to the cationic lipid membranes during the self-assembling of template, one can expect that the insertion of QDs should not destabilize the 3D organization. Many experiments were performed varying parameters such as the membrane surface charge, the concentration ratio QDs/actin, and the F-buffer concentration. The best experimental conditions were identified to improve the reproducibility (10 samples) as followed (Figure 2a): the actin polymerization buffer was not necessary in order to observe actin polymerization as previously observed under cationic lipid monolayers.[18] The surface charge has to be increased with a lipid mixture DMTAP/DMPC (2:8). The observation of a 3D order is very sensitive to a low QDs concentration (1 μmol/L) since an increase to 2.5 μmol/L generates a less ordered phase (Figure 3) composed of QDs chains embedded within lipid bilayers and actin filaments. The formation of actin−QDs−lipids complexes required two days and the samples are stable more than one month at room temperature when they are stored in capped capillaries (Figure 2b).

Regarding their structural analysis, the composite phase consists of strongly birefringent macroscopic fibers and exhibits an intense green fluorescence (Figure 2c,d). Powder diffraction obtained

dx.doi.org/10.1021/nl203216q |*Nano Lett.* 2011, 11, 5443–5448

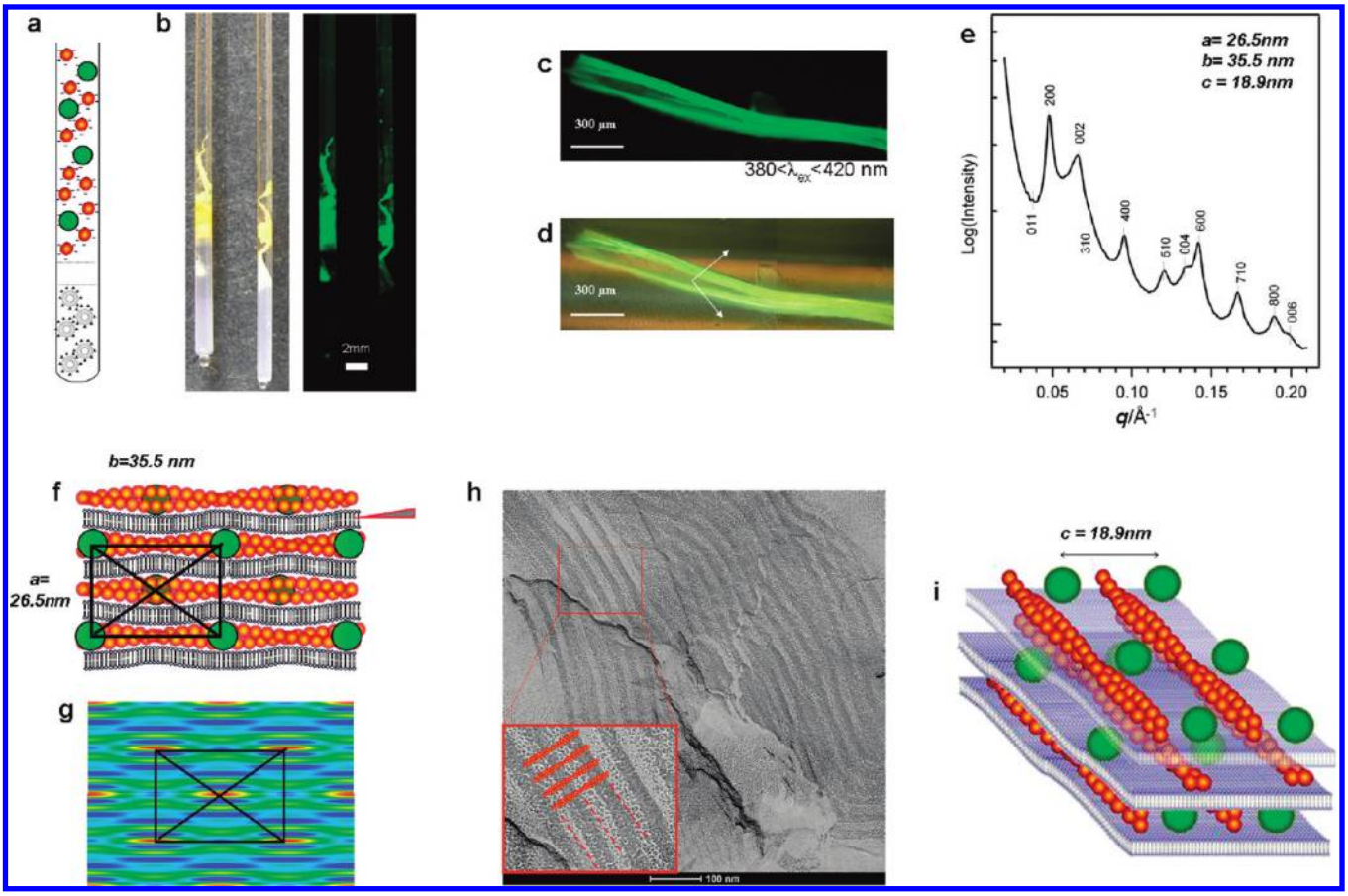

Figure 2. Structural characterization of the 3D crystal composed of quantum-dots embedded within F-actin microfilaments layers alternating with lipid membranes obtained by contact between 15 μL of DMTAP/DMPC (2:8) small unilamellar vesicles (20 mg/mL), 120 μL of a solution of G-actin (12 μmol/L), and a solution of functionalized quantum dots (1 μmol/L). (a) Sample preparation by contact between the two colloidal solutions (actin/QDs and vesicles) in a capillary (sketch not at the scale). (b) Optical observation by digital camera illuminated by white light (left) and UV light (right). (c,d) Morphologies observed by fluorescence and polarization microscopy. (e) Powder diffraction observed by SAXS experiments performed with a 3 m sample−detector distance at SWING@SOLEIL and the corresponding peak indexations in a 3D centered orthorhombic lattice. The HWHM of the Bragg peaks (<0.004 Å^{-1}) shows a positional order larger than 3000 Å. (f) Schematic view of the structure. Strong electrostatic interactions between anionic microfilaments and cationic lipids results in large undulations of the lipid bilayers. Red wedge indicates the freeze fracture plane. (g) Electron density projection on the (a,b) plane reveals quantum dots localization (red) and aliphatic chain oscillation (cyan). (h) Freeze fracture electron microscopy between the lipid bilayers shows one kind of corrugation. Actin microfilaments are drawn as scale reference. (i) Schematic sketch of the 3D organization.

by SAXS experiments exhibits Bragg peaks that can be indexed in an orthorhombic lattice (table in Supporting Information S8 and Figure 2e) with the three lattice parameters of a = 35.5 nm, b = 26.5 nm, and c = 18.9 nm. Only the (h,k,l) peaks satisfying to $h + k + l = 2n$ (with n an integer) were observed. This is in agreement with a body-centered orthorhombic lattice. These cell parameters are closed from that of the actin/lipid template alone suggesting that the hybrid QD/actin/lipid organization derives from the template structure. The large changes in the relative peak intensities confirm that the QD is embedded in the unit cell. Because the QD electron density is much larger than the one of organic template, the observed X-ray diffraction mainly finds its origin from the QD superstructure and gives access to the quality of the QD crystal. The sharpness of the Bragg peaks demonstrates the long-range positional order of QDs in the crystal (Figure 2e). The hydrophilic QDs can only be located in the channels delimited by two adjacent lipid membranes and two neighboring actin filaments. QDs are expected to be located in contact with the thinner part of the channel that is defined by the actin filament helix (Figure 2f) in order to reduce Coulomb repulsions between anionic QDs and actin. The QDs are not close to each other in the unit cell because this would produce an additional diffuse scattering due to pair interactions between disordered QDs as observed in the presence of a large excess of QDs (Figure 3c,d). The QDs localization is confirmed by electron density reconstruction (Figure 2g). Complementary freeze fracture electron microscopy images (Figure 2h) exhibit only one mode of membrane undulations with a repetition distance of around 35 ± 5 nm, which is induced by the helical modulation of the actin filaments along the a direction. The magnitude of the membrane undulation is enhanced by the QDs locations which are precisely located in the groove of the filaments (Figure 2f). Thus QDs have been incorporated within a template during its self-assembling process (Scheme 1). The three-dimensional order of the template is preserved during the inclusion of the QDs and results in a three-dimensional crystal of QDs (Figure 2i). When the concentration ratio between the QDs and the actin in solution is increased, one can observe a hybrid lamellar phase

dx.doi.org/10.1021/nl203216q |*Nano Lett.* 2011, 11, 5443–5448

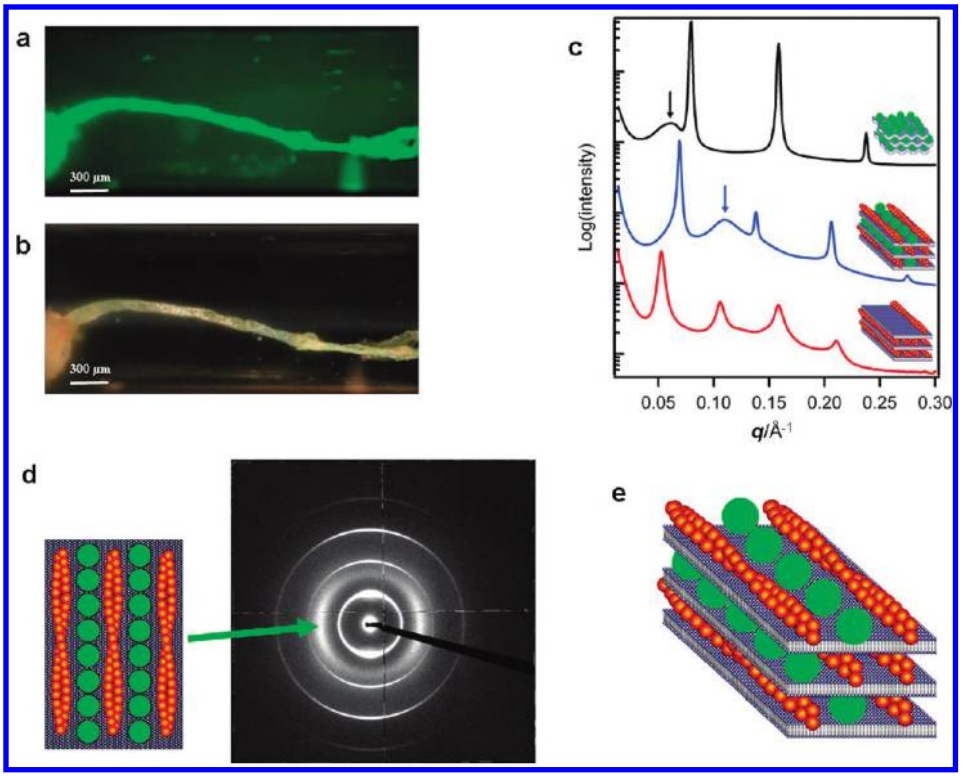

Figure 3. (a,b) Morphologies observed by fluorescence and polarization microscopy. (c) Powder diffraction (blue) observed by SAXS experiments performed at SWING@SOLEIL. Quantum dots/lipids complexes (Supporting Information 9) and actin/lipids complexes (Supporting Information 7) are shown for comparison. (d) Fiber diffraction observed by SAXS experiments performed with a 3 m sample−detector distance at SWING@SOLEIL. (e) Schematic sketch of the 3D organization.

including chains of close-packed QDs forced by the presence of actin (Figure 3).

In order to evaluate the relationship between fluorescent properties and QDs organizations, we investigate fluorescence spectra of different arrays of QDs (Figure 4a). Indeed, fluorescent properties of dyes are generally related to their aggregation states.[22] In the case of the 3D crystal of QDs, a fluorescence red shift of around 13 nm (53 meV) is observed. This shift is only obtained for the 3D crystal organization. The chemical environment composed of actins and lipids cannot explain such a shift. Indeed only a slight red shift of 2 nm (8 eV) was observed for chains of close-packed QDs embedded within membranes and actin filaments (Figure 3). As a complementary control, QDs embedded within bilayers[15] exhibits the same fluorescence spectrum than a suspension of isolated QDs. In the literature, a fluorescence red shift observed in linear chains[23] or 3D crystals[24] of close-packed QDs (interdistance below 2 nm) is attributed to fluorescence resonance energy transfer (FRET) between QDs. In the present case, FRET cannot explain the results because the QDs interdistances are larger than 10 nm, which is much higher than the Förster radius (5−7 nm).[25] Long range interactions generating energy lowering as observed in bacterial photosynthetic light harvesting systems[26] can also give rise to such a fluorescence red shift. Such behavior, called superradiance,[27] has been observed with QDs with an interdistance as long as 150 nm.[8] To test this hypothesis, fluorescence spectra were recorded in different area of the fiber. All spectra exhibit a fluorescence intensity that is directly related to the fluorescence shift in the 3D crystal area (Figure 4b,c). All spectra are the sum of two contributions: one due to the isolated QD and the other one due to a new fluorescent state. The contribution of the second one increases linearly with the total intensity of the peak and therefore can be directly attributed to the emergence of a unique new fluorescent state (Figure 4b,c and Supporting Information S10). This new fluorescence state observed within the 3D array is consistent with a superradiant emission that is characterized by slight energy loss (<5%) due to the fluorescence wavelength and a large increase (300%) of the fluorescence intensity.[28,29] The latter result illustrates the possibility to generate new optical properties with larger interdistances between QD within an ordered assembly.

Bottom-up methods are generally restricted to self-assembly in solution where the 3D array symmetry is imposed by the shape and the functionalization of nanoparticles.[11] The method reported here describes the inclusion of the quantum dots occurring during the self-assembling process of the bioorganic template. By mixing slowly different bioorganic and inorganic building blocks interacting through electrostatic interaction, we demonstrate the formation of a very well-defined 3D crystal of QDs. This strategy gives access to 3D arrays of nanoparticles whose original low symmetry[16] can reveal new physical properties. The fluorescence properties of the 3D crystals of quantum dots demonstrate a direct effect of the nanostructuration of the quantum dots within the crystal. The formation of 3D arrays of nanoparticles could open new route toward optical materials that are easily prepared by using self-assembling of vesicles, proteins, and hydrophilic nanoparticles in aqueous environment. This strategy could be extended to any kind of hydrophilic nanoparticles with various morphologies. Furthermore, the range of characteristic lengths can be extended by using another biological

dx.doi.org/10.1021/nl203216q |*Nano Lett.* 2011, 11, 5443–5448

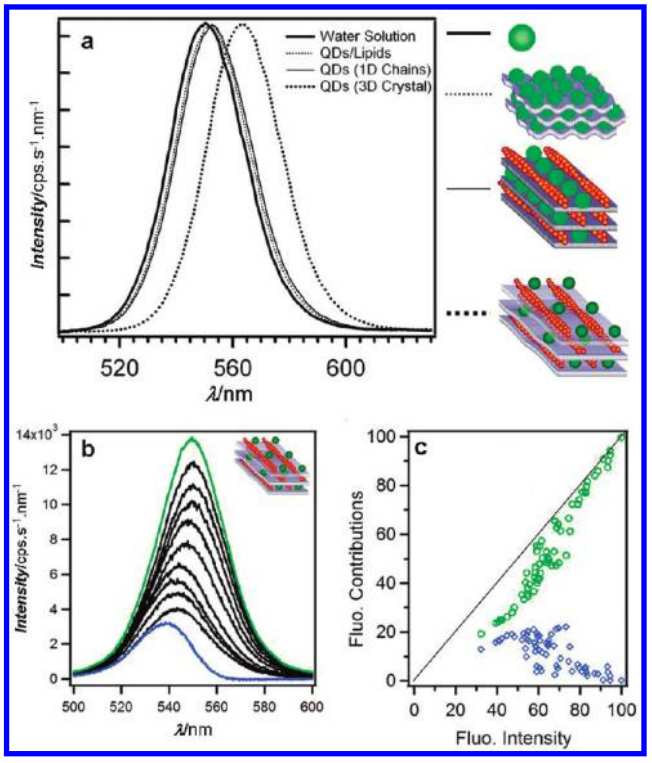

Figure 4. Emission spectra (ex = 405 nm) of varied quantum dots self-organizations. (a) A red shift depending on the type of self-organization is observed. The magnitude of the red shift is 13 nm (53 meV) in the case of the 3D arrays of quantum dots whereas the shift is only 2 ± 1 nm and 3 ± 1 nm in the case of low dimension structures in presence or not of actin. (b) Variation of fluorescence spectra of the 3D arrays of quantum dots. All spectra are the sum of two contributions due to the individual QDs fluorescence (blue) and a new fluorescent state (green) of which the respective intensities (green circles and blue diamonds of panel c) strongly depend on the total fluorescence intensity. For comparison, all intensities are normalized with respect to the maximal intensity (100). Note that the fluorescence intensity increase is mainly due to this new fluorescent state. All spectra and fits are shown in Supporting Information 10.

polyelectrolyte (DNA, microtubules, polysaccharides, amyloids fibers, and so forth) instead of actin filament.

■ ASSOCIATED CONTENT

Supporting Information. This section includes (1) materials and methods, (2) crystal structures of actin/lipid template obtained from SAXS experiments, (3) TEM images of lipid/quantum dots composite phase, and (4) raw fluorescence spectra of QD/lipid/actin composite phase. This material is available free of charge via the Internet at http://pubs.acs.org.

■ AUTHOR INFORMATION

Corresponding Author

*E-mail: (V.M.-A.) valerie.marchi-artzner@univ-rennes1.fr; (F.A.) franck.artzner@univ-rennes1.fr.

■ ACKNOWLEDGMENT

We are grateful for synchrotron radiation facilities from the ESRF and SOLEIL (no. SC2384 and 2008740), the ACI Nanoscience (no. NR0004), and Région Bretagne and Rennes Métropole for financial funding. We also thank Theyencheri Narayanan and Florian Meneau for high quality assistance in using Beamline ID02 and SWING, Tadeck Gulick for freeze fracture electron microscopy of actin lipid complexes, Anne Renault, Aurélie Parette, Loic Le Goff, and Cristelle Meriadec for preliminary experiments, and Robson Ferreira for helpful discussion on quantum dots luminescence.

■ REFERENCES

(1) Murray, C. B.; Kagan, C. R.; Bawendi, M. G. *Science* **1995**, *270*, 1335.
(2) Desvaux, C.; Amiens, C.; Fejes, P.; Renaud, P.; Respaud, M.; Lecante, P.; Snoeck, E.; Chaudret, B. *Nat. Mater.* **2005**, *4*, 750.
(3) Dumestre, F.; Chaudret, B.; Amiens, C.; Renaud, P.; Fejes, P. *Science* **2004**, *303*, 821.
(4) Courty, A.; Mermet, A.; Albouy, P. A.; Duval, E.; Pileni, M. P. *Nat. Mater.* **2005**, *4*, 395.
(5) Shevchenko, E. V.; Talapin, D. V.; Kotov, N. A.; O'Brien, S.; Murray, C. B. *Nature* **2006**, *439*, 55.
(6) Shevchenko, E. V.; Talapin, D. V.; Murray, C. B.; O'Brien, S. *J. Am. Chem. Soc.* **2006**, *128*, 3620.
(7) Abecassis, B.; Testard, F.; Spalla, O. *Phys. Rev. Lett.* **2008**, *100*, 115504.
(8) Scheibner, M.; Schmidt, T.; Worschech, L.; Forchel, A.; Bacher, G.; Passow, T.; Hommel, D. *Nat. Phys.* **2007**, *3*, 106.
(9) Lin, S.; Li, M.; Dujardin, E.; Girard, C.; Mann, S. *Adv. Mater.* **2005**, *17*, 2553.
(10) Kittel, C. *Introduction to Solid State Physics*, 8th ed.; Wiley: New York, 2004.
(11) Nie, Z. H.; Petukhova, A.; Kumacheva, E. *Nat. Nanotechnol.* **2010**, *5*, 15.
(12) Nykypanchuk, D.; Maye, M. M.; van der Lelie, D.; Gang, O. *Nature* **2008**, *451*, 549.
(13) Park, S. Y.; Lytton-Jean, A. K. R.; Lee, B.; Weigand, S.; Schatz, G. C.; Mirkin, C. A. *Nature* **2008**, *451*, 553.
(14) (a) Liang, H. J.; Angelini, T. E.; Ho, J.; Braun, P. V.; Wong, G. C. L. *J. Am. Chem. Soc.* **2003**, *125*, 11786. (b) Huang, Y.; Chiang, C.-Y.; Lee, S. K.; Gao, Y.; Hu, E. L.; Yoreo, J. D.; Belcher, A. M. *Nano Lett.* **2005**, *5* (7), 1429–1434.
(15) Dif, A.; Henry, E.; Artzner, F.; Baudy-Floc'h, M.; Schmutz, M.; Dahan, M.; Marchi-Artzner, V. *J. Am. Chem. Soc.* **2008**, *130*, 8289.
(16) Pouget, E.; Dujardin, E.; Cavalier, A.; Moreac, A.; Valery, C.; Marchi-Artzner, V.; Weiss, T.; Renault, A.; Paternostre, M.; Artzner, F. *Nat. Mater.* **2007**, *6*, 434.
(17) Dif, A.; Boulmedais, F.; Pinot, M.; Roullier, V.; Baudy-Floc'h, M.; Coquelle, F. M.; Clarke, S.; Neveu, P.; Vignaux, F.; Leborgne, R.; Dahan, M.; Gueroui, G.; Marchi-Artzner, V. *J. Am. Chem. Soc.* **2009**, *131*, 14738–14746.
(18) Renault, A.; Lenne, P. F.; Zakri, C.; Aradian, A.; Venien-Bryan, C.; Amblard, F. *Biophys. J.* **1999**, *76*, 1580.
(19) Wong, G. C. L.; Tang, J. X.; Lin, A.; Li, Y. L.; Janmey, P. A.; Safinya, C. R. *Science* **2000**, *288*, 2035.
(20) Zantl, R.; Artzner, F.; Rapp, G.; Radler, J. O. *Europhys. Lett.* **1999**, *45*, 90.
(21) Artzner, F.; Zantl, R.; Rapp, G.; Radler, J. O. *Phys. Rev. Lett.* **1998**, *81*, 5015.
(22) Tretiak, S.; Mukamel, S. *Chem. Rev.* **2002**, *102*, 3171.
(23) Tang, Z. Y.; Kotov, N. A. *Adv. Mater.* **2005**, *17*, 951.
(24) Kagan, C. R.; Murray, C. B.; Bawendi, M. G. *Phys. Rev. B* **1996**, *54*, 8633.
(25) Clapp, A. R.; Medintz, I. L.; Mauro, J. M.; Fisher, B. R.; Bawendi, M. G.; Mattoussi, H. *J. Am. Chem. Soc.* **2004**, *126*, 301.
(26) Monshouwer, R.; Abrahamsson, M.; vanMourik, F.; vanGrondelle, R. *J. Phys. Chem. B* **1997**, *101*, 7241.
(27) Dicke, R. H. *Phys. Rev.* **1954**, *93*, 99.
(28) Allen, L.; Elerby, J. H. In *Optical Resonance and Two-Level Atoms*; Dover: New York, 1987; p 174.
(29) Rehler, N. E.; Eberly, J. H. *Phys. Rev. A* **1971**, *3*, 1735.